



Unraveling the Density and Hardness of Sintered Hydroxyapatite: A Conclusive Comparison of Laboratory-Synthesized Versus Commercial Variants

Rizal Fauzuddin Noor Ramdhani ¹, Bagas Haqi Arrosyid ^{2,3}, Alfian Noviyanto ^{1,3,*}



¹ Department of Mechanical Engineering, Faculty of Engineering, Mercu Buana University, Jakarta, Indonesia

² Department of Engineering Physics, Faculty of Industrial Technology, Institut Teknologi Bandung, Bandung, Indonesia

³ Center of Excellence Advanced Materials, Nano Center Indonesia, Tangerang Selatan, Indonesia

* Corresponding author: alfian.noviyanto@mercubuana.ac.id

<https://doi.org/10.14710/jksa.28.3.130-137>

Article Info

Article history:

Received: 03rd December 2024

Revised: 04th April 2025

Accepted: 09th April 2025

Online: 30th April 2025

Keywords:

Density; Hydroxyapatite;

Hardness; Sintering

Temperature

Abstract

Hydroxyapatite (HA) is a bioceramic widely utilized in the medical field as a substitute for bone and dental applications. The mechanical properties of HA are influenced by its microstructure, which varies based on the source of the material, whether it is commercially acquired or laboratory-synthesized. This study aims to investigate and compare the properties of commercially available HA with those of laboratory-synthesized HA, as well as their mixtures, focusing on density and hardness. To conduct this investigation, both laboratory-synthesized and commercial HA were sintered at temperatures of 800°C, 900°C, 1000°C, and 1100°C for a duration of two hours. Additionally, various mixtures of the two sources of HA were prepared in weight percent ratios of 0:100, 30:70, 50:50, 70:30, and 100:0 using a planetary ball mill, also for two hours. The density of sintered HA was determined using Archimedes' principle, while its hardness was evaluated using a Vickers hardness tester. The findings revealed that laboratory-synthesized HA sintered at 1100°C exhibited the highest density and hardness, measuring 3.15 g/cm³ and 488.9 MPa, respectively. This superior performance can be attributed to the smaller particle size of the laboratory-synthesized HA, which enhances densification. The dense structure of the laboratory-synthesized HA results in reduced porosity and smaller grain sizes, as evidenced by scanning electron microscopy images. In contrast, the commercial HA achieved a density of only 3.00 g/cm³ at the same sintering temperature of 1100°C, attributable to poorer densification and a resultant porous microstructure. Notably, the mixture of commercial and laboratory-synthesized HA at a ratio of 30:70 demonstrated properties closely aligned with those of pure laboratory-synthesized HA, achieving a density of 3.14 g/cm³ and a hardness of 477.3 MPa. These results underscore the importance of source material and processing conditions in determining the mechanical properties of hydroxyapatite.

1. Introduction

Hydroxyapatite (HA) is a calcium phosphate compound with the chemical formula Ca₁₀(PO₄)₆(OH)₂. It is known for its biocompatibility, bioactivity, and similarity to the mineral components of human bones and teeth [1]. These properties make HA a prominent material in biomedical applications, particularly in bone grafts, dental implants, and prosthetic coatings, where it

enhances osseointegration [2, 3, 4, 5]. HA has a wide range of applications beyond the biomedical field. It is utilized in various non-biomedical areas, including as a catalyst, in chromatography, and as a filler in polymer composites [6]. Its stability and multifunctional properties make HA a valuable material in these applications.

Commercial HA is generally produced through industrial processes that utilize elevated temperatures to ensure a uniform composition and consistent particle size. However, the high-temperature production methods can present certain challenges, including the risk of partial decomposition, crystallinity alterations, and impurities, such as secondary phases like tricalcium phosphate. These factors can impact its mechanical properties and limit its adaptability for specific applications [7].

In contrast, laboratory-synthesized HA can be tailored using various chemical methods, such as wet precipitation, sol-gel, and hydrothermal synthesis. These methods allow for precise particle size, morphology, and stoichiometry control. Laboratory-synthesized HA also enables the addition of dopants, such as magnesium or zinc, to enhance its biological and mechanical performance. However, laboratory-synthesis methods can present challenges such as batch-to-batch variability and potential contamination, which may affect consistency compared to commercial HA [8, 9].

The performance of HA-based materials is subject to a range of influential factors, including microstructure, purity, and mechanical properties such as hardness. These properties are significantly affected by the method of HA fabrication, whether it is produced commercially or synthesized in the laboratory. Additionally, particle size plays a crucial role in determining the mechanical characteristics of the material [10]. Research conducted by Indra *et al.* [11] indicates that combining micron-sized HA with nano-sized HA can enhance material strength. This improvement is attributed to the ability of nano-sized particles to fill the pores within micron-sized HA, thereby increasing the overall density and mechanical strength of the composite.

The sintering temperature is another critical factor affecting the mechanical strength of HA. It can be adjusted based on HA particle size, with smaller particles requiring lower sintering temperatures. For instance, the appropriate sintering temperature for nano-sized HA is 1000°C using spark plasma sintering [12], while micron-sized HA may necessitate temperatures as high as 1250°C [13, 14]. Although micron-sized HA is less expensive, the challenge of high sintering temperatures remains. On the other hand, nano-sized HA offers the benefits of lower sintering temperatures and enhanced mechanical strength, though it is more costly to produce [15, 16].

Table 1. Reported sintering temperature and type of HA

Type of HA	Parameter	
	Sintering temp. (°C)	Mixing ratio (wt.%)
n-HA: μ -HA [15]	1000, 1050, 1100, 1150, 1200	80:20
HA: Flour [17]	900	30:70, 40:60, 50:50, 60:40, and 70:30
HA: Chitosan [18]	900	30:40, 40:60, 50:50, 60:40, and 70:30
HA [19]	700, 800, 900	N.A.

Despite extensive studies on HA applications, there is limited research comparing the effects of commercial and laboratory-synthesized HA on the microstructure and hardness of composite materials. While some studies focus on the biological or chemical behavior of these two types of HA, their mechanical aspects—particularly the role of HA sources (commercial vs. laboratory-synthesized) in influencing the process-structure-property relationship—remain underexplored. Systematic studies on the influence of HA sources on microstructural features such as grain size, porosity, phase distribution, and their impact on hardness are still scarce. Table 1 summarizes previous studies focusing on the effect of temperature and particle size on HA hardness but does not include a direct comparison between commercial and laboratory-synthesized HA.

This study aims to investigate and compare the characteristics of commercially available HA with laboratory-synthesized HA and their mixtures, with a primary focus on density and hardness. Addressing this knowledge gap is vital for optimizing material performance and customizing HA-based products for advanced engineering and biomedical applications.

2. Experimental

2.1. Materials

The HA utilized in this study was sourced from commercially available suppliers through Tokopedia and laboratory synthesis. Additionally, an examination of mixtures of these HAs was conducted, with detailed information regarding the composition presented in Table 2.

2.2. Procedure

The research methodology involves several critical stages: sample preparation, mixing, compaction, sintering, and characterization, as illustrated in Figure 1. Two types of HA were blended according to the composition outlined in Table 2. This mixing process was conducted using a planetary ball mill (PBM) at a speed of 100 RPM for two hours, utilizing a Teflon jar and steel balls for effective milling. Following the mixing stage, pellets were formed employing a compaction machine under a pressure of 2 tons, resulting in pellets with a diameter of 15 mm and an average thickness of 4 mm. Subsequently, these pellets were subjected to sintering at various temperatures—800°C, 900°C, 1000°C, and 1100°C—with a holding time of two hours at each specified temperature.

Table 2. Sample name and composition

Sample name	Composition (wt.%)	
	Commercial	Laboratory synthesized
Synthesis	0	100
30:70	30	70
50:50	50	50
70:30	70	30
commercial	100	0

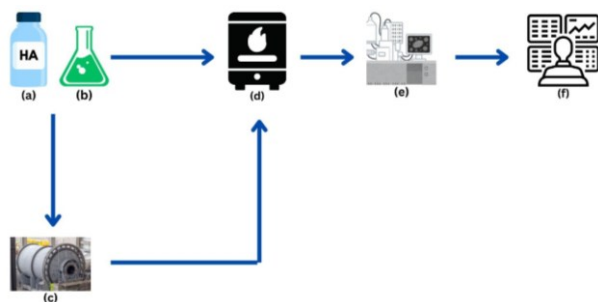


Figure 1. A schematic illustration of the research procedure. (a) and (b) depict the commercial and laboratory-synthesized HA, respectively. The HA powder was subjected to sintering within (d) a muffle furnace.

For comparative analysis, both samples in (a) and (b) were combined through (c) ball milling for 2 hours. Subsequently, the sintered samples were subjected to (e) characterization and further (f) analysis

2.3. Characterization

The particle sizes of commercially available and laboratory-synthesized HA were determined using a particle size analyzer (PSA). The density of the samples was assessed using the Archimedes method, which utilized deionized water as the medium. Additionally, microstructural characteristics were examined through scanning electron microscopy (SEM) to evaluate grain size and microstructure in relation to varying sintering temperatures. Moreover, Fourier transform infrared spectroscopy (FTIR) was employed for functional group analysis to understand the chemical alterations caused by changes in temperature. The crystalline phases of HA were analyzed through X-ray diffraction (XRD), with observed diffraction peaks compared to a reference database. Additionally, a Vickers hardness tester, utilizing an indentation load of 0.2 kgf, was employed to evaluate the hardness of the HA materials. The Vickers hardness test was determined using Equation 1.

$$H = 1.8544 \frac{F}{d^2} \tag{1}$$

Where, H represents hardness (MPa), F denotes load (N), and d is the average measurement of the two diagonals of the indentation (mm). This methodology enabled a comprehensive assessment of the impact of sintering temperature on the hardness properties of the samples.

3. Results and Discussion

Particle size measurements were conducted using PSA to evaluate the particle size distribution of laboratory-synthesized and commercial HA. The average particle size of laboratory-synthesized HA was found to be 313 nm, whereas that of commercial HA was 521 nm, as shown in Figure 2. Laboratory-synthesized HA displayed a sharper peak near smaller particle sizes (313 nm), indicating a more uniform particle size distribution. Conversely, commercial HA exhibited a broader distribution with a peak at a larger particle size (521 nm), reflecting more significant variability in particle size.

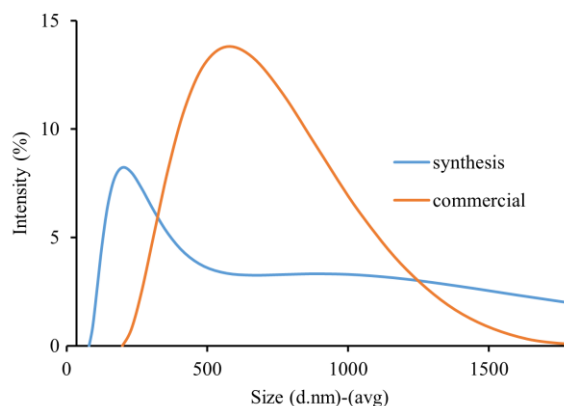


Figure 2. Particle size distribution graph for HA

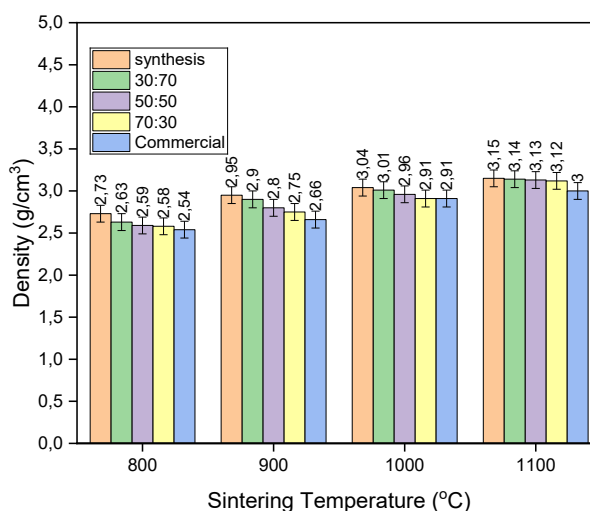


Figure 3. Density of HA at sintering temperature

The characteristic small particle size and homogeneous distribution of laboratory-synthesized HA can be attributed to the controlled synthesis process [4]. In contrast, large-scale production often requires elevated temperatures, leading to an increase in particle size. Differences in particle size significantly influence material properties such as density, porosity, and mechanical strength. Smaller particles (laboratory-synthesized HA) are generally more reactive during sintering, enabling densification at lower temperatures. In contrast, larger particles (commercial HA) may require higher sintering temperatures but offer lower production costs due to simpler manufacturing processes. Combining these two types of HA at different ratios provides opportunities to optimize both mechanical and economic properties.

Figure 3 illustrates the density of HA after sintering at varying temperatures (800°C, 900°C, 1000°C, and 1100°C) for 2 hours. The density measurements, performed using the Archimedes method, reveal that laboratory-synthesized HA consistently exhibited higher density than commercial HA across all sintering temperatures. Densities increased with higher sintering temperatures, attributable to densification and the corresponding reduction in porosity.

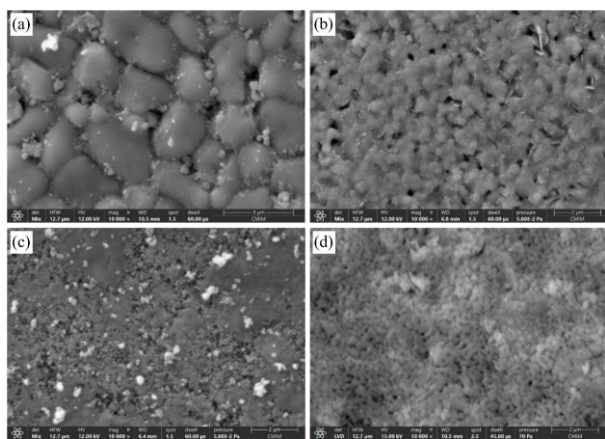


Figure 4. SEM images of sintered HA for (a) synthesized HA at 800°C, (b) synthesized HA at 900°C, (c) synthesized HA at 1100°C, and (d) commercial HA at 1100°C

At a sintering temperature of 1100°C, laboratory-synthesized HA achieved the highest density of 3.15 g/cm³, marginally exceeding that of commercial HA, which is 3.12 g/cm³. The blends of commercial and laboratory-synthesized HA in ratios of 30:70, 50:50, and 70:30 exhibited similar trends, demonstrating an increase in density as the sintering temperatures increased. This phenomenon suggests that the smaller particles from the laboratory-synthesized HA effectively occupy the voids in the larger particles of commercial HA, thereby enhancing overall densification. These findings align with existing literature, which indicates that smaller particles generally display higher sintering reactivity, resulting in greater densities at lower sintering temperatures [15, 20]. Achieving higher material densities necessitates uniform mixing and precise temperature control during the sintering process. These elements are critical, as they significantly affect grain distribution and the degree of material shrinkage [21, 22].

Figure 4 illustrates the microstructural observations of HA as seen through SEM images after sintering at varying temperatures: 800°C, 900°C, and 1100°C. Additionally, it provides a comparison between laboratory-synthesized and commercial HA. Figure 4(a) displays the microstructure of the laboratory-synthesized HA sintered at 800°C. At this temperature, the particles have not achieved full densification, resulting in most of them remaining isolated and exhibiting considerable porosity. This insufficient temperature hinders optimal densification, while excessive grain growth occurs.

The microstructure exhibits enhanced densification at a sintering temperature of 900°C (Figure 4(b)). The particles begin to interconnect, reducing porosity compared to the microstructure observed at 800°C. This temperature marks the initial stages of sintering, characterized by the formation of necks between particles. The development of these necks indicates that diffusion between the particles has occurred without the presence of abnormal grain growth, as shown at 800°C.

However, densification remains incomplete at this stage, as it represents an intermediate point in the

sintering process. This highlights the critical influence of temperature on reducing porosity and enhancing material density [23, 24]. The microstructure of the laboratory-synthesized HA shows markedly improved densification at 1100°C (Figure 4(c)). Most pores are closed, and the particles are tightly bonded together. Grain growth becomes more pronounced, leading to a denser and more uniform microstructure. At this elevated temperature, optimal material diffusion occurs, facilitating pore shrinkage and increased density. Such microstructures are generally associated with enhanced mechanical properties, including improved strength and hardness [25].

Under the same sintering conditions, the microstructure of commercial HA (Figure 4(d)) exhibits notable differences compared to that of laboratory-synthesized HA (Figure 4(c)). While densification has occurred in both cases, the microstructure of commercial HA retains a greater number of small pores. This is likely a result of the less uniform particle size distribution found in commercial HA, which impacts the sintering process. The presence of larger particles in commercial HA requires more energy to achieve optimal densification, leading to incomplete pore filling at the given temperature [20, 26].

Figure 5 illustrates the FTIR spectra of HA samples, emphasizing the characterization of functional groups in both laboratory-synthesized and commercial HA, as well as the influence of sintering temperatures (800, 900, 1000, and 1100°C) on laboratory-synthesized HA. The primary absorption bands observed indicate the presence of key functional groups, such as phosphate (PO₄³⁻), carbonate (CO₃²⁻), and hydroxyl (OH⁻), which are characteristic of HA's structure [27].

In the wavenumber range of 960–1100 cm⁻¹, prominent peaks associated with the symmetric and asymmetric stretching vibrations of phosphate ions (PO₄³⁻) are clearly observable. The intensity of these peaks increases with rising sintering temperatures, indicating an improvement in the material's crystallinity. This enhancement is attributed to enhanced material diffusion at elevated temperatures, which facilitates the formation of a more organized crystalline HA structure [28, 29]. Additionally, absorption bands in the 1400–1500 cm⁻¹ range and around 870 cm⁻¹ correspond to carbonate ions (CO₃²⁻), indicating their substitution within the HA structure. The intensity of these carbonate bands diminishes as the sintering temperature increases, suggesting that carbonate groups decompose at higher temperatures. This finding is consistent with existing literature indicating that carbonate ions tend to decompose during high-temperature sintering [13, 30].

At approximately 630 cm⁻¹, a strong absorption band is noted, representing the hydroxyl group (OH⁻), which is a distinguishing feature of HA. The intensity of this hydroxyl band is greater at lower sintering temperatures but decreases at higher temperatures, likely due to thermal desorption or decomposition reactions occurring at elevated temperatures. The FTIR spectrum of commercial HA exhibits relatively weaker peak

intensities than laboratory-synthesized HA, particularly regarding phosphate groups (PO_4^{3-}). This observation suggests that commercial HA may have lower crystallinity or a higher content of amorphous phases than laboratory-synthesized HA, especially following high-temperature sintering, which enhances the crystalline structure of laboratory-synthesized HA.

Figure 6 presents the XRD patterns of HA samples, highlighting the significant impact of the sintering process on the crystal structure and degree of crystallinity of the material. The XRD spectra in Figure 6 reveal distinct diffraction peaks characteristic of the hydroxyapatite phase, with dominant peaks observed at 2θ positions of approximately 31.8° , 32.2° , and 33.0° . These correspond to the (211), (112), and (300) crystallographic planes, as referenced from the ICDD 01-072-1243 database. For laboratory-synthesized HA without sintering, the diffraction peak intensities are lower, and the peaks are broader, indicating smaller crystallite sizes and a lower degree of crystallinity, corresponding to the crystallite size of 166 Å. Comparatively, commercial HA has a crystallite size of 405 Å. The crystallite size was determined utilizing the Scherrer equation (2) [31].

$$D = \frac{K\lambda}{B \cos \theta} \quad (2)$$

In Equation (2), D represents the crystallite size, K is the shape factor, commonly assumed to be 0.9, B denotes the width (full width at half maximum, FWHM) of the XRD peak expressed in radians, and θ is the Bragg angle. As the sintering temperature increases, a notable rise in the intensity of the diffraction peaks is observed, accompanied by a narrowing of these peaks. This phenomenon indicates the growth of crystallites and an enhancement in crystallinity. The crystallite size of laboratory-synthesized HA consistently increases with higher sintering temperatures. Specifically, at sintering temperatures of 800, 900, 1000, and 1100°C, the crystallite sizes measured were 266, 379, 480, and 531 Å, respectively.

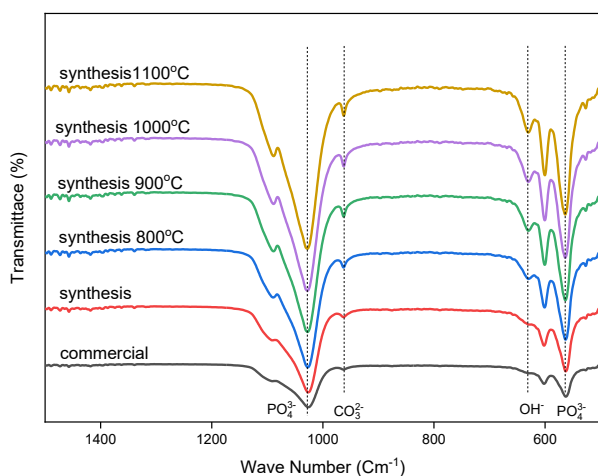


Figure 5. FTIR spectra of sintered HA at various temperatures, including the HA before sintering for both synthesized and commercial samples

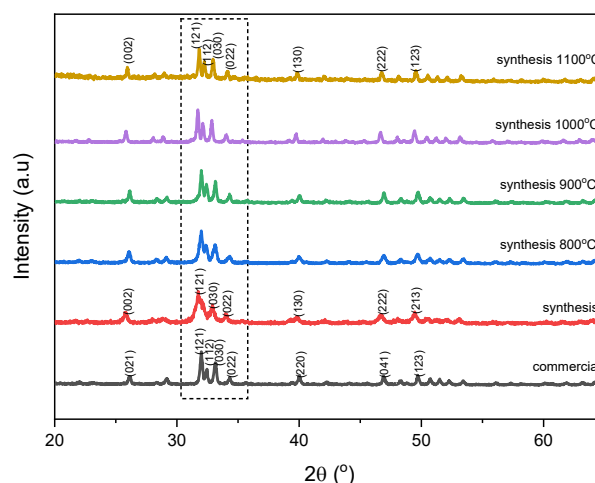


Figure 6. XRD patterns of synthesized HA as a function of temperature. For comparison, XRD patterns of both synthesized and commercial HA were included

Additionally, XRD patterns indicate that the crystal structure of HA is hexagonal, with a space group designation of $P 6_3/m$. This hexagonal arrangement is indicative of the highly ordered atomic structure characteristic of HA, while the identification of this specific space group confirms the presence of six-fold rotational symmetry and a mirror plane that is perpendicular to the c -axis. At a sintering temperature of 1100°C, the diffraction peaks exhibit the highest intensities and the lowest FWHM, reflecting a more ordered and homogeneous crystal structure [32].

The hardness testing results for HA, as shown in Figure 7, demonstrate that material hardness is significantly influenced by both the sintering temperature and the mixing ratio of laboratory-synthesized and commercial HA. For laboratory-synthesized HA, the hardness increased from 152.2 MPa at a sintering temperature of 800°C to 488.9 MPa at 1100°C. This increase reflects a direct relationship between sintering temperature and material hardness, where higher temperatures enable better material densification and reduced porosity. These findings are consistent with previous studies that show increasing sintering temperatures improve the mechanical properties of materials, including hardness [33, 34].

However, other studies have reported that excessive sintering temperatures may result in reduced mechanical strength due to excessive grain growth and the formation of microcracks in the material structure [35]. In this study, the maximum sintering temperature of 1100°C resulted in increased hardness without any indications of mechanical degradation. Compared to human bone, the hardness of laboratory-synthesized HA sintered at 1100°C is observed to fall within the range characteristic of human bone hardness. The hardness of human bone varies by type, typically ranging from 279 MPa to 501 MPa [36, 37]. To improve the mechanical properties of HA, it is common to incorporate reinforcement materials [38, 39, 40].

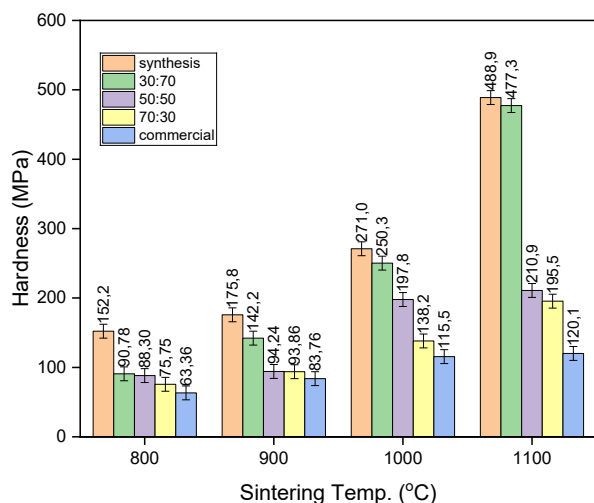


Figure 7. Hardness results of sintered HA at different compositions and sintering temperatures

In addition to sintering temperature, the mixing ratio of laboratory-synthesized to commercial HA also affects hardness. At 1100°C, the 30:70 ratio achieved the highest hardness of 477.3 MPa, surpassing the 50:50 and 70:30 ratios, which reached 210.9 and 195.5 MPa, respectively. This indicates that the source of HA contributes to improved material density by filling the pores present in commercial HA. Moreover, even at a lower sintering temperature (900°C), the 30:70 ratio achieved a hardness of 142.2 MPa, which is higher than the hardness of commercial HA at a sintering temperature of 1100°C. These findings are consistent with the literature, indicating that smaller particles positively increase hardness by reducing porosity and enhancing material density [11, 41].

4. Conclusion

This study demonstrates that hydroxyapatite (HA) characteristics, both laboratory-synthesized and commercial, are significantly influenced by particle size, mixing ratios, and sintering temperature. Laboratory-synthesized HA exhibits smaller particle sizes, measuring 313 nm, compared to commercially available HA, which measures 521 nm, as determined by particle size analysis. The different sources of HA yield varying results in terms of density; specifically, at a sintering temperature of 1100°C, laboratory-synthesized HA achieves the highest density of 3.15 g/cm³, surpassing that of commercial HA, which reaches a density of 3.12 g/cm³. SEM images illustrate that laboratory-synthesized HA exhibits a dense microstructure, whereas the commercial counterpart displays a porous microstructure. This disparity in microstructure contributes to a considerable difference in hardness. Laboratory-synthesized HA achieves an impressive hardness of 488.9 MPa at 1100°C, while commercial HA attains only 120.1 MPa at the same sintering temperature. Combining both types of HA in a 30:70 ratio yields enhanced densification, resulting in a density of 3.14 g/cm³ and a hardness of 477.3 MPa. Overall, laboratory-synthesized HA demonstrates significant advantages in terms of density, crystallinity, and hardness compared to commercial HA. Combining synthesized and commercial HA offers a balanced

approach to cost and performance, positioning it as a superior material for biomedical applications.

Acknowledgments

The authors are grateful to the Nano Center Indonesia for providing the research facilities.

References

- [1] Fifi Afifah, Sari Edi Cahyaningrum, Sintesis dan karakterisasi hidroksiapatit dari tulang sapi (*Bos Taurus*) menggunakan teknik kalsinasi, *UNESA Journal of Chemistry*, 9, 3, (2020), 189-196 <https://doi.org/10.26740/ujc.v9n3.p189-196>
- [2] Sergey V. Dorozhkin, Bioceramics of calcium orthophosphates, *Biomaterials*, 31, 7, (2010), 1465-1485 <https://doi.org/10.1016/j.biomaterials.2009.11.050>
- [3] Sudip Mondal, Sumin Park, Jaeyeop Choi, Thi Thu Ha Vu, Vu Hoang Minh Doan, Truong Tien Vo, Byeongil Lee, Junghwan Oh, Hydroxyapatite: A journey from biomaterials to advanced functional materials, *Advances in Colloid and Interface Science*, 321, (2023), 103013 <https://doi.org/10.1016/j.cis.2023.103013>
- [4] N. A. S. Mohd Pu'ad, R. H. Abdul Haq, H. Mohd Noh, H. Z. Abdullah, M. I. Idris, T. C. Lee, Synthesis method of hydroxyapatite: A review, *Materials Today: Proceedings*, 29, (2020), 233-239 <https://doi.org/10.1016/j.matpr.2020.05.536>
- [5] Elisa Fiume, Giulia Magnaterra, Abbas Rahdar, Enrica Verné, Francesco Baino, Hydroxyapatite for Biomedical Applications: A Short Overview, *Ceramics*, 4, 4, (2021), 542-563 <https://doi.org/10.3390/ceramics4040039>
- [6] Samar J. Kalita, Abhilasha Bhardwaj, Himesh A. Bhatt, Nanocrystalline calcium phosphate ceramics in biomedical engineering, *Materials Science and Engineering: C*, 27, 3, (2007), 441-449 <https://doi.org/10.1016/j.msec.2006.05.018>
- [7] Brigitte Wopenka, Jill D. Pasteris, A mineralogical perspective on the apatite in bone, *Materials Science and Engineering: C*, 25, 2, (2005), 131-143 <https://doi.org/10.1016/j.msec.2005.01.008>
- [8] M. Bilton, A. P. Brown, S. J. Milne, Sol-gel synthesis and characterisation of nano-scale hydroxyapatite, *Journal of Physics: Conference Series*, 241, 1, (2010), 012052 <https://doi.org/10.1088/1742-6596/241/1/012052>
- [9] Iain R. Gibson, 1.3.4A - Natural and Synthetic Hydroxyapatites, in: W.R. Wagner, S.E. Sakiyama-Elbert, G. Zhang, M.J. Yaszemski (Eds.) *Biomaterials Science (Fourth Edition)*, Academic Press, 2020, <https://doi.org/10.1016/B978-0-12-816137-1.00023-4>
- [10] Xuan Cai, Hua Tong, Xinyu Shen, Weixuan Chen, Juan Yan, Jiming Hu, Preparation and characterization of homogeneous chitosan-poly(lactic acid)/hydroxyapatite nanocomposite for bone tissue engineering and evaluation of its mechanical properties, *Acta Biomaterialia*, 5, 7, (2009), 2693-2703 <https://doi.org/10.1016/j.actbio.2009.03.005>
- [11] Ade Indra, Ridwan Firdaus, Ismet Hari Mulyadi, Jon Affi, Gunawarman, Enhancing the physical and mechanical properties of pellet-shaped

- hydroxyapatite by controlling micron- and nano-sized powder ratios, *Ceramics International*, 46, 10, Part B, (2020), 15882-15888
<https://doi.org/10.1016/j.ceramint.2020.03.136>
- [12] Yusuf Wibisono, Ni Luh Bella Dwijaksana, Wahyu Bambang Widayatno, Agus Sukarto Wismogroho, Muhamad Ikhlasul Amal, Nurul Taufiqu Rochman, Toshiyuki Nishimura, Alfian Noviyanto, Synthesis and Sinterability of Hydroxyapatite from Fishery by-products, *Journal of Korean Ceramic Society*, 55, 6, (2018), 570-575
<https://doi.org/10.4191/kcers.2018.55.6.03>
- [13] Mohammad Zulhasif Ahmad Khiri, Khamirul Amin Matori, Mohd Hafiz Mohd Zaid, Che Azurahaman Che Abdullah, Norhazlin Zainuddin, Ibrahim Mustapha Alibe, Nadia Asyikin Abdul Rahman, Siti Aisyah Abdul Wahab, Aisyah Zakiah Khirel Azman, Nuraidayani Effendy, Crystallization behavior of low-cost biphasic hydroxyapatite/ β -tricalcium phosphate ceramic at high sintering temperatures derived from high potential calcium waste sources, *Results in Physics*, 12, (2019), 638-644
<https://doi.org/10.1016/j.rinp.2018.12.025>
- [14] G. Muralithran, S. Ramesh, The effects of sintering temperature on the properties of hydroxyapatite, *Ceramics International*, 26, 2, (2000), 221-230
[https://doi.org/10.1016/S0272-8842\(99\)00046-2](https://doi.org/10.1016/S0272-8842(99)00046-2)
- [15] Ade Indra, Gunawarman, Jon Affi, Ismet Hari Mulyadi, Yogi Wiyanto, Physical and mechanical properties of hydroxyapatite ceramics with a mixture of micron and nano-sized powders: optimising the sintering temperatures, *Ceramics-Silikáty*, 65, 3, (2021), 224-234
<https://doi.org/10.13168/cs.2021.0022>
- [16] S. Ramesh, K. L. Aw, R. Tolouei, M. Amiriyan, C. Y. Tan, M. Hamdi, J. Purbolaksono, M. A. Hassan, W. D. Teng, Sintering properties of hydroxyapatite powders prepared using different methods, *Ceramics International*, 39, 1, (2013), 111-119
<https://doi.org/10.1016/j.ceramint.2012.05.103>
- [17] Izmi Mahfudi, Joko Triyono, Teguh Triyono, Karakterisasi biokomposit *sheep hydroxyapatite* (sha)/shellac/tepung terigu, *Mekanika: majalah ilmiah mekanika*, 17, 2, (2018), 44-48
<https://doi.org/10.20961/mechanika.v17i2.35125>
- [18] Junaidi Rasid, Joko Triyono, Teguh Triyono, Karakterisasi Material Biokomposit Bovine Hidroksapatit (BHA)/Shellac dan Kitosan Sebagai Material Bone Filler, *ROTASI*, 19, 2, (2017), 82-87
<https://doi.org/10.14710/rotasi.19.2.82-87>
- [19] Md. Sahadat Hossain, Monika Mahmud, Sazia Sultana, Mashrafi Bin Mobarak, M. Saiful Islam, Samina Ahmed, Coupled effect of particle size of the source materials and calcination temperature on the direct synthesis of hydroxyapatite, *Royal Society Open Science*, 8, 9, (2021), 210684
<https://doi.org/10.1098/rsos.210684>
- [20] M. Safarzadeh, Chin Fei Chee, S. Ramesh, M. N. Ahmad Fauzi, Effect of sintering temperature on the morphology, crystallinity and mechanical properties of carbonated hydroxyapatite (CHA), *Ceramics International*, 46, 17, (2020), 26784-26789
<https://doi.org/10.1016/j.ceramint.2020.07.153>
- [21] Alfian Noviyanto, Dang-Hyok Yoon, Rare-earth oxide additives for the sintering of silicon carbide, *Diamond and Related Materials*, 38, (2013), 124-130
<https://doi.org/10.1016/j.diamond.2013.07.003>
- [22] Alfian Noviyanto, Seung-Woo Han, Hyun-Woo Yu, Dang-Hyok Yoon, Rare-earth nitrate additives for the sintering of silicon carbide, *Journal of the European Ceramic Society*, 33, 15, (2013), 2915-2923
<https://doi.org/10.1016/j.jeurceramsoc.2013.05.017>
- [23] M. N. Rahaman, 2 - Kinetics and mechanisms of densification, in: Z.Z. Fang (Ed.) *Sintering of Advanced Materials*, Woodhead Publishing, 2010,
<https://doi.org/10.1533/9781845699949.1.33>
- [24] Randall M. German, *Liquid Phase Sintering*, Springer New York, New York, 1985,
<https://doi.org/10.1007/978-1-4899-3599-1>
- [25] E. Saiz, L. Gremillard, G. Menendez, P. Miranda, K. Gryn, A. P. Tomsia, Preparation of porous hydroxyapatite scaffolds, *Materials Science and Engineering: C*, 27, 3, (2007), 546-550
<https://doi.org/10.1016/j.msec.2006.05.038>
- [26] Sung-Min Lee, Suk-Joong L. Kang, Theoretical analysis of liquid-phase sintering: Pore filling theory, *Acta Materialia*, 46, 9, (1998), 3191-3202
[https://doi.org/10.1016/S1359-6454\(97\)00489-8](https://doi.org/10.1016/S1359-6454(97)00489-8)
- [27] Yusuf Wibisono, Syifa Navisa, Dinda Kiswara Arofah, Mochamad Bagus Hermanto, Alfian Noviyanto, Saiful, Tonni Agustiono Kurniawan, Comparative study of physical properties of hydroxyapatite derived from Asian moon scallop and batik shells using sol-gel techniques for producing inorganic membrane plate, *Chemical Papers*, 78, 12, (2024), 7125-7139
<https://doi.org/10.1007/s11696-024-03592-2>
- [28] Md. Sahadat Hossain, Samina Ahmed, FTIR spectrum analysis to predict the crystalline and amorphous phases of hydroxyapatite: a comparison of vibrational motion to reflection, *RSC Advances*, 13, 21, (2023), 14625-14630
<https://doi.org/10.1039/d3ra02580b>
- [29] José Reyes-Gasga, Esmeralda L. Martínez-Piñeiro, Galois Rodríguez-Álvarez, Gaby E. Tiznado-Orozco, Ramiro García-García, Etienne F. Brès, XRD and FTIR crystallinity indices in sound human tooth enamel and synthetic hydroxyapatite, *Materials Science and Engineering: C*, 33, 8, (2013), 4568-4574
<https://doi.org/10.1016/j.msec.2013.07.014>
- [30] Atchara Khamkongkao, Thanachai Boonchuduang, Wantana Klysubun, Penphitcha Amonpattaratkit, H. thaichnok Chunate, Nutth Tuchinda, Adulphan Pimsawat, Sujittra Daengsakul, Pitphichaya Suksangrat, Wutthigrai Sailuam, Drusawin Vongpramate, Atipong Bootchanont, Boonrat Lohwongwatana, Sintering behavior and mechanical properties of hydroxyapatite ceramics prepared from Nile Tilapia (*Oreochromis niloticus*) bone and commercial powder for biomedical applications, *Ceramics International*, 47, 24, (2021), 34575-34584
<https://doi.org/10.1016/j.ceramint.2021.08.372>
- [31] P. Scherrer, Bestimmung der inneren Struktur und der Größe von Kolloidteilchen mittels Röntgenstrahlen, in: *Kolloidchemie Ein Lehrbuch*, Springer Berlin Heidelberg, Berlin, Heidelberg, 1912,
https://doi.org/10.1007/978-3-662-33915-2_7
- [32] Sandra M. Londoño-Restrepo, Mariana Herrera-Lara, Leon R. Bernal-Alvarez, Eric M. Rivera-

- Muñoz, Mario E. Rodríguez-García, In-situ XRD study of the crystal size transition of hydroxyapatite from swine bone, *Ceramics International*, 46, 15, (2020), 24454-24461
<https://doi.org/10.1016/j.ceramint.2020.06.230>
- [33] S. Ramesh, N. S. Virik, L. T. Bang, A. Niakan, C. Y. Tan, J. Purbolaksono, Boon Kar Yap, W. D. Teng, Sintering behaviour of forsterite-doped hydroxyapatite ceramics, *Ceramics-Silikáty*, 59, 2, (2015), 181-186
- [34] Onur Yontar, Mevlüt Gürbüz, Mechanical Properties of Dense Artificial Bone Fabricated by Powder Processing, *International Journal of Multidisciplinary Studies and Innovative Technologies*, 3, 1, (2019), 22-24
- [35] Marta Trzaskowska, Vladyslav Vivcharenko, Agata Przekora, The Impact of Hydroxyapatite Sintering Temperature on Its Microstructural, Mechanical, and Biological Properties, *International Journal of Molecular Sciences*, 24, 6, (2023), 5083
<https://doi.org/10.3390/ijms24065083>
- [36] Sheng Li, Jian-zhao Wang, Bing Yin, Zu-sheng Hu, Xiao-juan Zhang, Wei Wu, Guo-bin Liu, Ya-ke Liu, Lei Fu, Ying-ze Zhang, Atlas of Human Skeleton Hardness Obtained Using the Micro-indentation Technique, *Orthopaedic Surgery*, 13, 4, (2021), 1417-1422
<https://doi.org/10.1111/os.12841>
- [37] Bing Yin, Jia-liang Guo, Jian-zhao Wang, Sheng Li, Ya-ke Liu, Ying-ze Zhang, Bone Material Properties of Human Phalanges Using Vickers Indentation, *Orthopaedic Surgery*, 11, 3, (2019), 487-492
<https://doi.org/10.1111/os.12455>
- [38] Ying Cao, Tianshu Shi, Chen Jiao, Huixin Liang, Ruoyu Chen, Zongjun Tian, Anchao Zou, Youwen Yang, Zhen Wei, Changjiang Wang, Lida Shen, Fabrication and properties of zirconia/hydroxyapatite composite scaffold based on digital light processing, *Ceramics International*, 46, 2, (2020), 2300-2308
<https://doi.org/10.1016/j.ceramint.2019.09.219>
- [39] Mariana F. Vassal, J. Nunes-Pereira, Sónia P. Miguel, Ilídio J. Correia, Abílio P. Silva, Microstructural, mechanical and biological properties of hydroxyapatite - CaZrO₃ biocomposites, *Ceramics International*, 45, 7, Part A, (2019), 8195-8203
<https://doi.org/10.1016/j.ceramint.2019.01.122>
- [40] Renata Nunes Jardim, Anderson Araújo Rocha, Alexandre Malta Rossi, Aline de Almeida Neves, Maristela Barbosa Portela, Ricardo Tadeu Lopes, Thais Maria Pires dos Santos, Yutao Xing, Eduardo Moreira da Silva, Fabrication and characterization of remineralizing dental composites containing hydroxyapatite nanoparticles, *Journal of the Mechanical Behavior of Biomedical Materials*, 109, (2020), 103817
<https://doi.org/10.1016/j.jmbbm.2020.103817>
- [41] M. Aminzare, A. Eskandari, M. H. Baroonian, A. Berenov, Z. Razavi Hesabi, M. Taheri, S. K. Sadrnezhad, Hydroxyapatite nanocomposites: Synthesis, sintering and mechanical properties, *Ceramics International*, 39, 3, (2013), 2197-2206
<https://doi.org/10.1016/j.ceramint.2012.09.023>